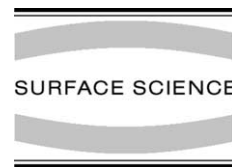




ELSEVIER

Surface Science 495 (2001) 173–184



www.elsevier.com/locate/susc

Change of magnetic property in ultrathin Fe films grown on Pd(1 1 1) induced by morphological change and interdiffusion

J.-H. Choi ^a, T.-U. Nahm ^{b,*}, Wookje Kim ^a, Wondong Kim ^a, J. Chung ^a,
J.-Y. Kim ^a, H. Koh ^a, S.-J. Oh ^a

^a Department of Physics and Center for Strongly Correlated Material Research, Seoul National University, Seoul 151-742, South Korea

^b Department of Physics, Hanyang University, Seoul 133-791, South Korea

Received 20 December 2000; accepted for publication 22 August 2001

Abstract

We have studied the magnetic and structural properties of ultrathin Fe films grown on a Pd(1 1 1) substrate using in situ surface magneto-optic Kerr effect (SMOKE), X-ray photoelectron spectroscopy (XPS), and low energy electron diffraction (LEED). SMOKE measurements show that perpendicular magnetic anisotropy was partially induced by post-annealing at 450 K for a 2.0 ML (monolayer, ML) film. For thicker (2.5 and 5.5 ML) films, a strong enhancement of the Kerr signal was observed upon post-annealing at temperatures above 600 K. Underlying reasons, such as morphological change and interdiffusion of Fe atoms into the Pd substrate, are discussed on the basis of the XPS and LEED results. © 2001 Elsevier Science B.V. All rights reserved.

Keywords: Magnetic phenomena (cyclotron resonance, phase transitions, etc.); X-ray photoelectron spectroscopy; Surface structure, morphology, roughness, and topography; Surface diffusion; Iron; Palladium; Magnetic films; Low index single crystal surfaces

1. Introduction

Ferromagnetic ultrathin surface layers and multilayers have been studied very extensively in the past two decades [1]. One reason for the interest in such systems is that perpendicular magnetic anisotropy (PMA) can be induced since the surface out-of-plane anisotropy can dominate over the bulk anisotropy. Many studies have been performed on various multilayer systems with the

aim to enhance PMA. In this respect, thin Fe films on various metal substrates have attracted particular interest. Fe/Ag(100) is one of the most studied systems that shows spin reorientation as a function of Fe film thickness [2,3] and post-annealing temperature [4–7], and it has been shown that Fe films on Cu(100) exhibit also very complex magnetic behavior which is correlated to their structure [8–13]: The Fe films have a face-centered tetragonal structure which is ferromagnetic below 5 ML. Between 6 and 11 ML, only the top two layers have tetragonal expansion, and the inner layers have an isotropic fcc structure, which is antiferromagnetic [14,15]. This leads to the observation of the oscillating behavior of the Kerr signal with thickness [11].

* Corresponding author. Tel.: +82-2-2290-0912; fax: +82-2-2295-6868.

E-mail address: tschnahm@hanyang.ac.kr (T.-U. Nahm).

Ferromagnetic thin films on a Pd substrate enjoy additional scientific interest since the magnetic moment of Pd atoms can be induced by ferromagnetic coupling with adjacent magnetic layers [16]. We have recently investigated ultrathin magnetic Co films on Pd(1 1 1) [17], in connection with the study of multilayered Co/Pd structures that display PMA [18] as well as large magneto-optical Kerr rotations in the ultraviolet spectral region [19].

In this paper, we investigate thin Fe film on Pd(1 1 1). With Fe being located next to Co in the periodic table, it should be very instructive to study the Fe/Pd system for reasons of comparison with the Co/Pd case. However, due to a large lattice mismatch of 4.2% between bcc Fe ($a = 2.87 \text{ \AA}$) and fcc Pd ($a = 3.89 \text{ \AA}$), and a lattice mismatch of even -8.4% between fcc Fe ($a = 3.59 \text{ \AA}$) and Pd, the epitaxy of the Fe/Pd(1 1 1) system should be very ambiguous and complex. For this reason, most of the studies on the Fe/Pd system have been performed with Pd(1 0 0) as a substrate [20–23], where the mismatch is reduced to only 3.3% for bcc Fe overlayers. The only previous study dealing with the morphology of Fe films on Pd(1 1 1) was performed with low energy electron diffraction (LEED) and Auger electron spectroscopy (AES) [24]. The growth mode was classified as complex and significantly changing with the substrate temperature, a flat surface was reportedly achieved for the first two atomic layers grown on a 450 K substrate. Such a complex epitaxy can affect the magnetic properties of ultrathin films.

The importance of morphology in surface magnetism have been noticed very early in this field [25], but a detailed understanding was not achieved until recently when changes in magnetic anisotropy resulting from morphological changes upon various annealing conditions were reported for Fe/Ag(1 0 0) [7] and for Fe/Cu(1 0 0) [26]. The growth mode of Fe on Ag(1 0 0) was classified as neither layer-by-layer nor Stranski–Krastanov [27], and the surface morphology was improved by either growing or post-annealing the films at elevated temperatures [28]. It was shown that such spin reorientations can be interpreted by taking roughness-induced dipolar surface anisotropy as well as surface anisotropy into account [7]. The

observed spin reorientation of Fe films grown at 100 K on Cu(1 0 0) upon annealing at 350 K was accompanied by considering smoothing of the Fe film surface, which is similar to the Fe/Ag(1 0 0) case [26].

In this study, changes of the surface magneto-optic Kerr effect (SMOKE) signal from Fe films of several monolayers (ML) thickness on Pd(1 1 1) upon annealing were studied with the aim to elucidate the effects of morphology on surface magnetism in the Fe/Pd(1 1 1) system. Especially, the 2.0 ML Fe case is of interest because this thickness corresponds roughly to the critical thickness of many thin film systems above which ferromagnetic ordering appears at room temperature (RT), and yet it is thin enough to possibly maintain PMA. This is also reportedly the very thickness where a flat surface was achieved by proper annealing processes [24]. Therefore, a significant change in the magnetic properties can be expected around this thickness. Thicker films (Fe 2.5 and 5.5 ML) were also studied for comparison. To investigate the morphological changes and the chemical environment, we used LEED and X-ray photoelectron spectroscopy (XPS).

In the following, we demonstrate that the change in surface magnetism upon annealing is caused by morphological changes as well as interdiffusion of Fe atoms into the Pd substrate. The structural and chemical changes after each annealing step are found to be complex. The PMA is only partially induced in the 2.0 ML Fe case upon annealing at 450 K due to a flattened surface, and an enhancement in SMOKE signal has been observed upon high temperature annealing, when interdiffusion of Fe atoms into Pd take place.

2. Experimental

The SMOKE, XPS, and LEED measurements were performed in a home-made ultrahigh vacuum (UHV) chamber. The base pressure of the chamber was 8×10^{-11} Torr. The Pd(1 1 1) substrate was of disk-type with 10 mm diameter and 1 mm thickness. The surface was cleaned by several cycles of Ar⁺ sputtering at 1 keV and annealing at 870 K in the UHV chamber until the crystal sur-

face showed a well-defined LEED pattern with no contamination detected in the XPS spectrum. The light source for SMOKE measurement was a 10-mW He–Ne laser with $\lambda = 623.8$ nm.

The XPS spectra shown here were obtained with unmonochromatized Mg K_{α} radiation with $h\nu = 1253.6$ eV. The overall resolution was 0.9 eV. Since the O Auger spectrum excited by Mg K_{α} lines partly overlaps with the loss structure of the Fe 2p photoemission (PE) lines, we also used Al K_{α} radiation with $h\nu = 1486.6$ eV to check O contamination on the surface. No contamination on Fe layers was detected for at least 3 h.

The Fe film was deposited on the Pd substrate at room temperature by an e-beam heating method. An iron wire of 99.99% purity was heated by electron bombardment from a tungsten filament. The film thickness was first calibrated using a quartz thickness monitor, and was then cross-checked by XPS using Fe 2p and Pd 3d core-level PE line intensities at sub-ML coverage assuming no island growth. The values obtained from these two methods agree with each other within an error of 10%. In this work, the Fe film thickness was represented in units of one monolayer and 1 ML was set as 1.32×10^{15} Fe atoms cm^{-2} , assuming a pseudomorphic growth of the Fe film on the Pd(111) surface.

The whole experiment proceeded as follows: First, Fe films of various thicknesses up to 4.5 ML were grown at RT, and SMOKE measurements were performed. Then we again prepared 2.0, 2.5, and 5.5 ML Fe films to study structure, morphological change, and magnetic properties before and after the post-annealing processes using SMOKE, XPS, and LEED.

3. Results and discussion

3.1. SMOKE results

In Fig. 1, longitudinal SMOKE signals of RT deposited Fe films of various thickness (2.0, 2.5, 3.5, and 4.5 ML) are presented. No polar signal was detected. Ferromagnetic hysteresis curves appeared in films thicker than 2.5 ML, and the critical thickness at RT could be assigned a value

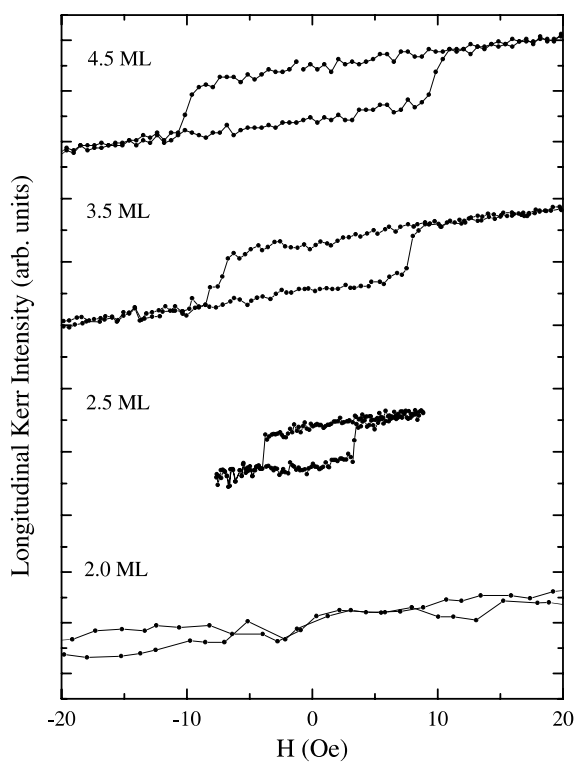


Fig. 1. Longitudinal Kerr signals from Fe films of different thickness.

between 2.0 and 2.5 ML. The coercivity increased accordingly as the film became thicker. This seems to be due to magnetic domain wall pinning in thicker disordered Fe overlayers. In the Fe/Pd(100) case, where almost layer-by-layer growth was observed up to 2 ML, the critical thickness at room temperature was between 1.3 and 1.7 ML [23]. Considering even some uncertainties with respect to thickness calibration, this value is very different from ours, suggesting some morphological difference between Fe films on Pd(100) and Pd(111).

Fig. 2 shows variation of the SMOKE signals from a 2.0 ML Fe film upon two different post-annealing situations. After RT deposition, no hysteresis loop can be observed for either longitudinal or polar directions, and thus an Fe film on Pd(111) is paramagnetic at RT up to this thickness. Upon 450 K annealing, hysteresis curves are observed for both directions, which indicates

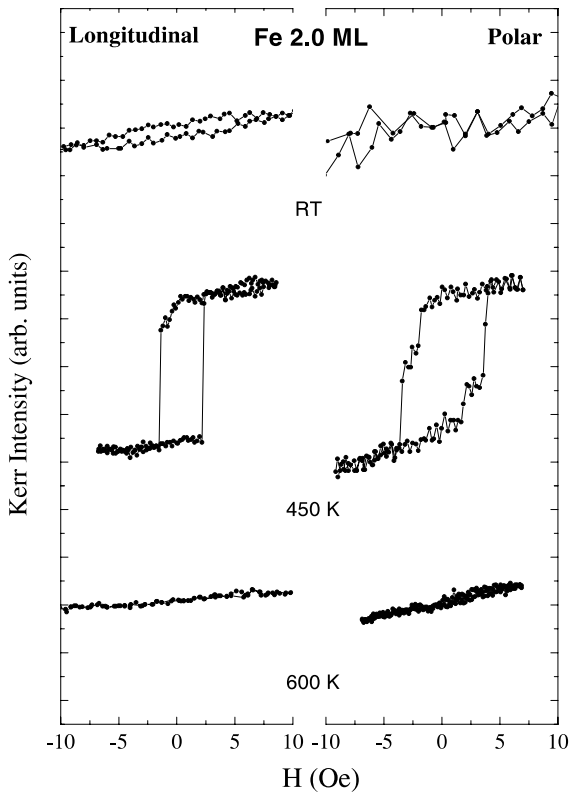


Fig. 2. Kerr signals from a 2.0 ML Fe film after RT deposition, upon 450 and 600 K post-annealing processes.

that the magnetization vector is canted. The co-existence of in-plane and out-of-plane hysteresis curves is commonly observed in systems which show spin reorientation [5,7,12,29]. The step in the polar Kerr signal is not real, but an artifact due to instrumental noise. Upon 600 K post-annealing, a hysteresis loop disappears again for both directions.

For thicker films, different behavior in Kerr signals is observed after post-annealing. The SMOKE results are shown in Fig. 3. Ferromagnetic Kerr signals in longitudinal direction are observed after RT deposition, but a polar signal could not be induced by any annealing process. Upon 600 K (660 K) post-annealing of a 2.5 ML (5.5 ML) film, there is an increase in coercivity as well as in Kerr intensity. Further annealing at 750 K leads to a reduction of coercivity for the 2.5 ML film. However, we cannot know the origin of these

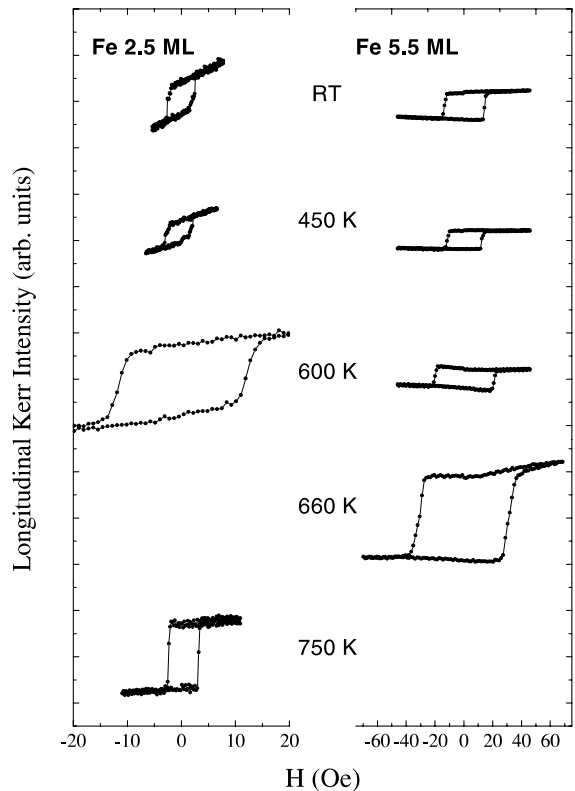


Fig. 3. Longitudinal Kerr signals from 2.5 and 5.5 ML Fe films prepared by RT deposition, upon 450, 600, 660, and 750 K post-annealing processes. Note the different magnetic field scales.

magneto-optical properties from the SMOKE results alone, and more discussion will follow after looking at the LEED and XPS results.

3.2. LEED results

At the end of the cleaning cycle of the Pd(1 1 1) substrate, the LEED pattern showed sharp (1×1) spots. However, evaporation of 2.0 ML of Fe completely blurred the pattern, probably due to disordered Fe atoms or island growth at the initial stage. Upon annealing at 450 K, the diffuse $p(1 \times 1)$ pattern becomes visible, suggesting a flattening and ordering effect of the process. This agrees with a previous suggestion from Auger intensity measurements [24] that a 2 ML Fe film grown on a 450 K Pd(1 1 1) substrate becomes flat.

After 600 K annealing, the spots become even sharper, which again must be due to the flattening of the surface as a whole or of the patches. All LEED patterns, however, show different qualitative I - V characteristics from each other. We also could not see any indication of ordered Fe(1 1 0) islands in bcc structure, which is expected on the basis of the large lattice mismatch.

From 2.5 and 5.5 ML films, we obtained similar LEED results, and it can be concluded that the annealing process flattens the surface of the film as a whole or of the patches, for the thickness and temperature range tested. This contrasts with the reported RT layer-by-layer growth of Fe atoms on Pd(1 0 0) [23], where lattice mismatch is smaller.

3.3. XPS results

Figs. 4 and 5 show the changes of the Fe 2p and Pd 3d XPS spectra of a 2.0 ML Fe film upon annealing. The spectra of various annealing stages

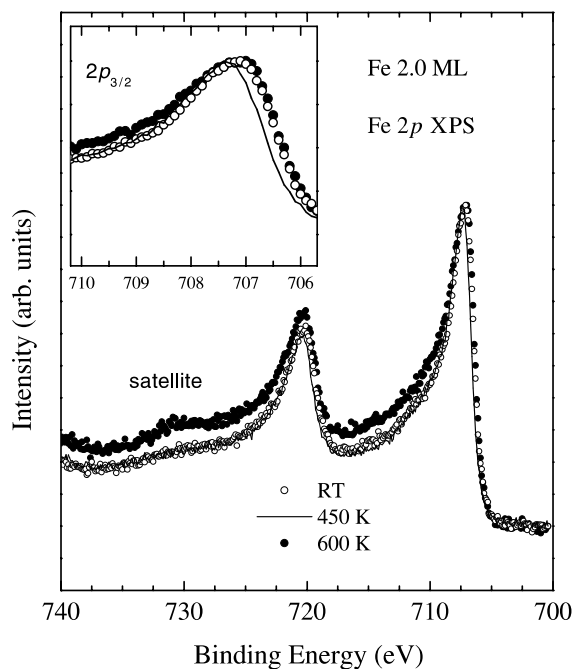


Fig. 4. Fe 2p XPS spectra of Fe 2.0 ML film after room temperature deposition (open circles), upon 450 K post-annealing (solid line), and upon 600 K post-annealing (filled circles). The inset shows $2p_{3/2}$ peaks in a narrow region.

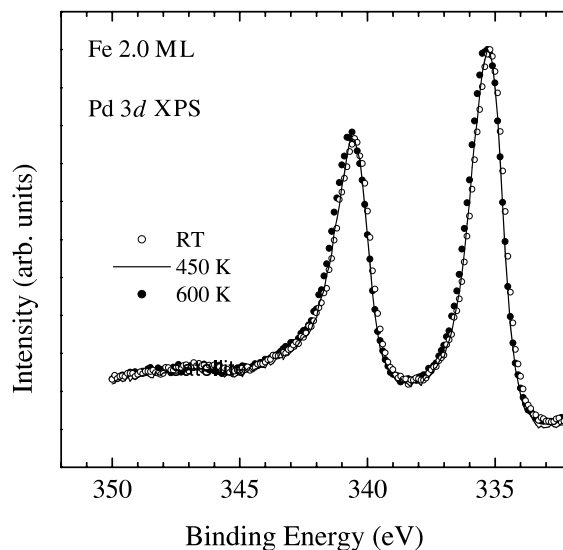


Fig. 5. Pd 3d XPS spectra of a 2.0 ML Fe film after RT deposition (open circles), upon 450 K post-annealing (solid line), and upon 600 K post-annealing (filled circles).

are shown together to compare the linewidths and the binding energies. For 2.5 and 5.5 ML of Fe, the spectra are shown separately (Figs. 6 and 7). Finally, we show in Fig. 8 the relative change of Fe 2p and Pd 3d peak intensities upon annealing at different temperatures. In addition, the peak intensity ratios between Fe 2p and Pd 3d are listed in Table 1. Although the estimation of the absolute peak intensities has about a 10% error due to the arbitrariness in background removal and due to the slight change in photon flux, the errors of the relative intensities in Table 1 have far less value because the errors in both sides cancel each other out.

3.3.1. 2.0 ML Fe film

For a 2.0 ML Fe film, it can be seen that the width of the Fe $2p_{3/2}$ peak varies depending on the annealing temperatures (Fig. 4). The width has a minimum value when the film is annealed at 450 K. This reduction in the width compared with that of the RT grown sample can be considered as the result of flattening, because flattened film could be associated with relatively uniform chemical environments for Fe atoms compared with island growth or disordered cases. This explanation is

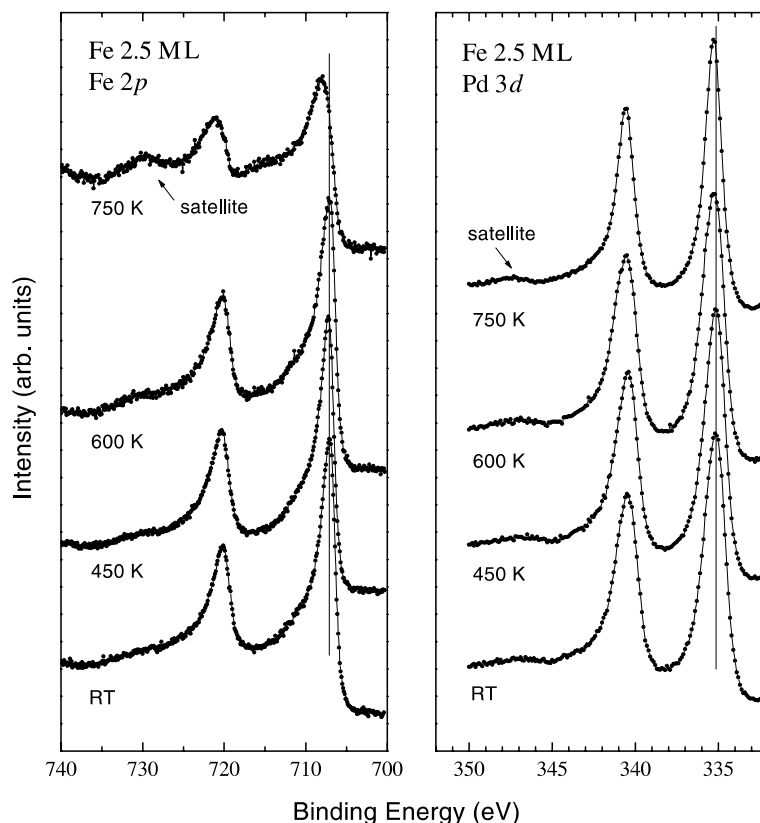


Fig. 6. Fe 2p and Pd 3d XPS spectra of 2.5 ML after RT deposition, and upon annealings at 450, 600, and 750 K. The vertical lines mark the peak positions of Fe 2p_{3/2} and Pd 3d_{5/2} PE lines for the as-deposited case.

also supported by a slight increase of the Fe 2p peak intensity (Fig. 8).

Upon 600 K annealing, both Fe 2p and Pd 3d peaks are broadened and the peak intensity ratio is decreased having nearly the same value as the as-deposited case (Table 1). We can think of several reasons for this observation: the partial dewetting of Fe patches or the interdiffusion of Fe atoms into the substrate or both of them. If only dewetting occurred, Fe atoms should form island patches whose chemical environment is more or less similar to that of Fe bulk. This requires that the Fe 2p spectrum should resemble that of bulk Fe, which is not the case in Fig. 4. On the other hand, interdiffusion is a more probable explanation because Fe–Pd alloys are miscible over the whole composition range [30]. In addition, the satellite structure

of the Fe 2p_{1/2} PE line at a binding energy of around 731 eV becomes large, which may reflect the dilution of Fe in the Pd substrate. A similar behavior had been observed in the satellite intensity change of Ni 2p levels of Ni–Pd alloys [31]. However, if this were the only process that happened, the Fe 2p peaks should be shifted towards the higher binding energy side as in annealed 2.5 ML Fe film (Fig. 6), which again is not the case. From this reasoning, we can conclude that part of the flattened Fe layers on Pd(1 1 1) form islands by dewetting, and part of the Fe atoms diffuse into the Pd substrate and form local surface alloys. This can also qualitatively explain the observed LEED I - V characteristics which are different both for the 450 K annealed surface and for the as-deposited surface.

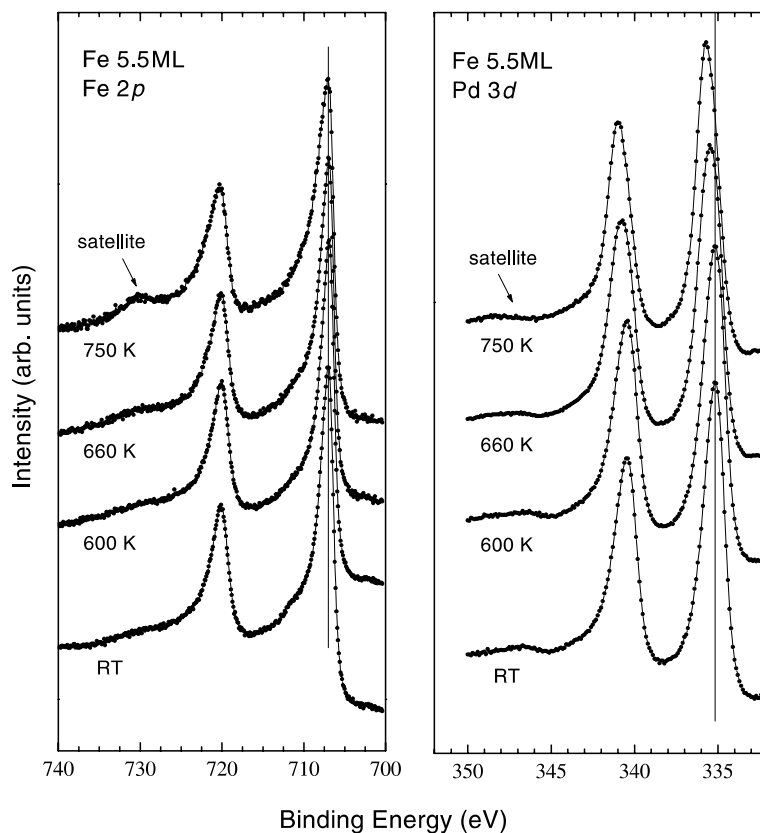


Fig. 7. Fe 2p and Pd 3d XPS spectra of 5.5 ML after RT deposition, and upon annealings at 600, 660, and 750 K. The vertical lines mark the peak positions of Fe 2p_{3/2} and Pd 3d_{5/2} PE lines for the as-deposited case.

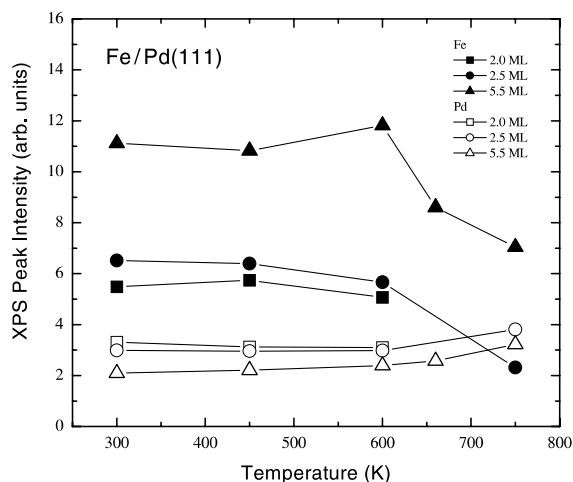


Fig. 8. Change of the XPS peak intensity upon annealing for 2.0 (squares), 2.5 (circles), and 5.5 (triangles) ML. Filled symbols refer to Fe 2p and open symbols to Pd 3d.

Table 1

Intensity ratios of Fe 2p relative to Pd 3d levels

	2.0 ML	2.5 ML	5.5 ML
RT deposition	1.66	2.18	5.32
450 K annealing	1.84	2.16	4.89
600 K annealing	1.63	1.90	4.94
660 K Annealing	–	–	3.34
750 K annealing	–	0.61	2.18

3.3.2. 2.5 ML Fe film

For the 2.5 ML Fe film (Fig. 6), the change in the Fe 2p PE lineshape is slightly different from the 2.0 ML case. Upon annealing at 450 K, the peak becomes sharper and is shifted towards higher binding energies as compared to the 2.0 ML case, but the size of the shift is reduced from +0.25 to +0.05 eV. There is virtually no change in XPS

peak intensity ratio upon 450 K annealing (Table 1). This implies that the Fe layer in the 2.5 ML case is not much flattened as compared to the 2.0 ML case. Upon further annealing at 600 K, the Fe $2p_{3/2}$ peak is broadened and shifted back to the peak position of the as-deposited case while the satellite structure is slightly enhanced. However, upon annealing at 750 K, the $2p_{3/2}$ peak is greatly broadened and shifted from 707.1 to 708 eV and the satellite of $2p_{1/2}$ is now clearly visible. These changes cannot be interpreted as oxide formation, because, there is no contamination detected and the binding energy of oxides are higher than 709 eV [32]. The Fe 2p peak intensity is reduced, while the Pd 3d peak intensity is enhanced. All of these observations can be explained by surface alloy formation resulting from interdiffusion of Fe atoms into the substrate.

In order to estimate the composition of the Fe concentration of the surface alloy $\text{Fe}_x\text{Pd}_{1-x}$, we use Johansson and Mårtensson's method for treating core-level binding-energy shifts in alloys [33–35]. This method is based on a Born–Haber cycle involving the heat of formation usually calculated after Miedema [36]. The Fe 2p binding-energy shift calculated in a simplified scheme [33] is $\Delta E = 0.12(1-x)$ eV, which is far smaller than the observed value. When we use the measured heat of formation of Fe in Pd [37], this relationship becomes $\Delta E = 0.6(1-x)$ eV. This indicates that Fe atoms are diluted in the Pd substrate.

This big change in the Fe 2p binding energy is also accompanied by the shift in Pd 3d peak position by +0.15 eV. Applying the same method to the Pd 3d binding-energy shift, we found that

$$\Delta E = 1.66x \text{ eV}, \quad (1)$$

as in Ref. [22], where ΔE is the Pd 3d binding-energy shift and x is the Fe concentration. Since $\Delta E = 0.15$ eV, we can estimate from Eq. (1) that the Fe concentration is 9%.

To confirm this result, we compare the photoelectron intensity ratio of 450 and 750 K annealed films. Since the photoelectrons emitted from the inner layers decay due to inelastic scattering [38,39], we can estimate the composition of Fe–Pd alloy layers. Assuming a pseudomorphic behavior

for the 450 K annealed film, the photoelectron intensity ratio is given by

$$\frac{I_{\text{Fe } 2p}}{I_{\text{Pd } 3d}} = A \times \frac{0.5 \sum_{n=0}^1 \exp(-nd/\lambda_{\text{Fe}}) + 0.5 \sum_{n=0}^2 \exp(-nd/\lambda_{\text{Fe}})}{0.5 \sum_{n=2}^{\infty} \exp(-nd/\lambda_{\text{Pd}}) + 0.5 \sum_{n=3}^{\infty} \exp(-nd/\lambda_{\text{Pd}})}, \quad (2)$$

where d is the interlayer spacing of Pd{111}. The electron inelastic mean free paths have the values $\lambda_{\text{Fe}} = 4.5$ ML and $\lambda_{\text{Pd}} = 5.9$ ML for Fe 2p and Pd 3d photoelectrons excited by Mg K α radiation [39]. The constant A represents the ratio of the photoionization cross-sections and the effect of analyzer transmission function. If we assume that the surface alloy forms homogeneously with sharp interface upon 750 K annealing, the photoelectron intensity ratio would be

$$\frac{I_{\text{Fe } 2p}}{I_{\text{Pd } 3d}} = A \times \frac{x \sum_{n=0}^{l-1} \exp(-nd/\lambda_{\text{Fe}})}{(1-x) \sum_{n=0}^{l-1} \exp(-nd/\lambda_{\text{Pd}}) + \sum_{n=l}^{\infty} \exp(-nd/\lambda_{\text{Pd}})}, \quad (3)$$

with the constraint

$$x \times l = 2.5,$$

where x is the Fe concentration and l is the thickness of surface alloy in monolayers. This gives $x = 0.15$, which is in agreement with the rough estimation using Johansson and Mårtensson's model. Since an Fe–Pd bulk alloy is known to show ferromagnetic ordering at RT for Fe compositions down to 12% [41], we believe 0.15 is the more correct estimation.

3.3.3. 5.5 ML Fe film

The same explanation can be applied to the 5.5 ML film (Fig. 7). Any significant change in the Fe 2p main peaks does not happen even upon 750 K annealing, and only a slight enhancement of the satellite intensity is visible. This small change may be expected because of the finite electron inelastic mean free path discussed above; for photoelectrons from the Fe 2p levels within a Pd(111) matrix, the mean free path is 4.5 ML [39]. This means that for thicker films, we cannot get full

information about the Fe atoms deep inside layers or islands.

However, the Pd 3d peak is shifted from the pure Pd(1 1 1) case by 0.32 and 0.57 eV upon 660 and 750 K annealing, respectively. This can be best understood by the formation of a Fe–Pd surface alloy resulting from Fe atom interdiffusion; using Eq. (1), we can estimate that the Fe composition of the surface alloy is about 34%, which is comparable to the RT as-deposited Fe/Pd(1 0 0) case [22]. To confirm this estimation, we calculated also the Fe concentration using Eq. (3). The result was $x = 0.39$, which is in good agreement. The absence of a Fe–Pd surface alloy on Pd(1 1 1) at RT is probably due to its close-packed surface structure. The 0.32 eV shift observed for the 660 K annealed layer is in fact due to the co-existence of two peaks, one for the above Fe–Pd alloy and the other for pure Pd(1 1 1).

The reduction and the shift of the satellite structure of Pd 3d_{3/2} PE peak also reflects the fact that there is some change in the electronic structure [40]. This interpretation is also in accordance with the change of peak intensity (Fig. 8), because interdiffusion will lead to a reduction of the Fe 2p peak intensity and an enhancement of the Pd 3d peak intensity.

Another piece of information we can get from a change in peak intensities is that there is some dewetting of the Fe layers upon 450 K annealing. While the Fe 2p peak intensity is reduced, the Pd 3d peak intensity is enhanced upon 450 K annealing. This is not an experimental artifact because the relative intensity ratio in Table 1, in which errors are expected to be largely cancelled by each other, also shows a reduction of the ratio between Fe 2p and Pd 3d peak intensities. The apparent enhancement of both peak intensities upon 600 K annealing seems to be due to the onset of interdiffusion.

Before discussing the relationship between magnetic and morphological changes upon annealing, we will shortly summarize LEED and XPS results for the 2.0, 2.5, and 5.5 ML Fe films. For the 2.0 and 2.5 ML films, post-annealing at 450 K flattens the surface. But further annealing at 600 K leads to partial dewetting and partial interdiffusion, and at 750 K, strong interdiffusion

occurs at least for the 2.5 ML film. For thicker film (5.5 ML), dewetting occurs at 450 K, and interdiffusion is followed after annealing at temperatures higher than 600 K.

4. Relation between SMOKE, LEED, and XPS results

4.1. 2.0 ML Fe film

From the preceding morphology study, we can characterize that a 2.0 ML Fe film post-annealed at 450 K is relatively flat without interdiffusion at the interface. For a 2.0 ML film, since we observed hysteresis loops both in longitudinal and polar directions, we can conclude that magnetic anisotropy is induced by a proper change in morphology. Similar results have been reported in other systems such as Fe/Cu(1 0 0) [26] and Fe/Ag(1 0 0) [7,12]. In the Fe/Cu(1 0 0) case, it was observed that there is an irreversible spin reorientation from a longitudinal to a polar direction for a 6 ML Fe film grown at 100 K, and it was concluded from STM measurement that reorientation was caused by smoothing the film surface. A similar explanation was given for the Fe/Ag(1 0 0) case. In both cases, the induction of PMA was observed at a thickness where longitudinal magnetic anisotropy was present before annealing. In our case, magnetic anisotropy both in the longitudinal and the polar direction was induced at the thickness where no ferromagnetic behavior was detected at RT, probably because of the small size of disordered Fe patches at RT. The induced PMA in all these cases can be interpreted as a result of an increase in surface anisotropy after post-annealing, the magnitude of which is more than enough to compensate the decrease in roughness-induced dipolar surface anisotropy [7].

Upon 600 K post-annealing, a ferromagnetic hysteresis loop was not observed in the 2.0 ML case, for which we conjectured that both dewetting and interdiffusion take place. In this case, the Fe islands, which seem to be more or less pseudomorphic to the Pd(1 1 1) substrate, are probably too small to order ferromagnetically. For Fe atoms of surface alloy, the disappearance may

seem strange because an Fe–Pd bulk alloy is ferromagnetic at RT for Fe compositions down to 12% [41]. If interdiffusion leads to Fe–Pd alloy formation whose Fe concentration is below this value, then the alloy film would be paramagnetic. Since 2.5 ML Fe film becomes ferromagnetic Fe–Pd surface alloy whose Fe concentration is about 14%, we can conclude that the surface alloy formed by annealing of 2.0 ML Fe film has a lower Fe concentration than this case.

4.2. 2.5 and 5.5 ML Fe films

In Fig. 3, enhancements of the Kerr signals for the 2.5 and 5.5 ML films were observed by more than 200% and 300%, respectively. There might have been some change in reflectivity upon post-annealing, but it is not probable that this reflectivity change alone caused such strong enhancements. For a Co–Pt(111) surface alloy, it has been estimated that reflectivity changes could explain only about one-third of the observed 300% enhancement of the Kerr signal [42].

Microscopically, the coupling between the electric field of light and the electron spin within a magnetic medium occurs through the spin–orbit interaction, and the Kerr effect manifests itself because of the unbalanced population of electron spins for ferromagnetic materials. Therefore, a change in the Kerr signal can result from changes in spin–orbit interaction in ferromagnetic materials [43]. In our case, an enhancement of the Kerr signal was observed simultaneously with the interdiffusion of Fe atoms. For the 2.5 ML film, the Kerr signal was enhanced upon a 600 K annealing step, and at the same time a significant reduction in the Fe 2p PE peak intensity occurred (Fig. 8). For the 5.5 ML film, only after the 660 K annealing, a simultaneous Kerr signal enhancement and a reduction in the Fe 2p PE peak intensity were observed. From these observations, we can conclude that in the 2.5 and 5.5 ML cases, the mechanism of enhancing the Kerr signal is closely related to the formation of a surface alloy as discussed in Ref. [42]. In previous calculations [44,45], spin–orbit coupling enhancement was expected in the cases of Fe or Co multilayers or intermetallics with Pd or Pt, which in turn affects the polar Kerr

rotations. The interdiffusion will cause part of the Fe atoms to be in contact with Pd atoms, which is different from the low temperature case, where only Fe atoms at the interface can be influenced by adjacent Pd atoms.

Another probable explanation is based on the enhanced magnetic moments of Fe and Pd, the latter being highly expected because of giant magnetic moment behavior in bulk alloys [46,47]. All of these might cause the huge change observed in Kerr rotation.

Fig. 3 also showed that post-annealing enhances coercivity as well as the Kerr signal intensity when interdiffusion occurs. This can be interpreted as a result of magnetic domain wall pinning, centers of which are largely removed by 750 K annealing.

In the 2.5 and 5.5 ML Fe film cases, a ferromagnetic Kerr signal in polar direction could not be detected upon annealing. The difference between 2.0 ML and thicker films can be explained by the thickness dependence of the magnetic anisotropy energy. From a phenomenological point of view, the critical thickness for PMA is between 2.0 and 2.5 ML, above which the volume anisotropy contribution outweighs the surface contribution and suppresses PMA.

5. Conclusions

To summarize, magnetic and morphological properties of ultrathin Fe films grown on a Pd(111) surface were investigated using SMOKE, LEED, and XPS. By combining the experimental results, the change in morphology by a suitable annealing process was shown to induce ferromagnetism in the Fe/Pd(111) system around a critical Fe film thickness of about 2 ML. A flat surface with a sharp interface could be achieved by 450 K post-annealing, and magnetizations both in longitudinal and in polar direction were concurrently induced. Further annealing at 600 K completely demagnetized the film because of dewetting and because of the onset of Fe-diluted surface alloy formation.

For thicker films, a different type of change of the Kerr signal was observed. There were only

longitudinal SMOKE signals after RT deposition, and no polar signal was detected. For a 5.5 ML film, annealing at 450 K leads to a slight dewetting of Fe layers. An enhancement of the Kerr signal was also observed upon annealing steps at 600 and 660 K for 2.5 and 5.5 ML, respectively, accompanied by a reduction in the relative XPS intensity ratio and an enhancement of the Fe 2p PE satellite peaks. These observations indicate the formation of surface alloy as a result of Fe interdiffusion. The Kerr signal was also enhanced in these cases.

These observations show that interdiffusion as well as morphological changes can affect the magnetic and magneto-optical properties of the Fe/Pd(111) systems.

Acknowledgements

This work was supported in part by the Ministry of Science and Technology (MOST) of Korea through the Future Basic Nanotechnology project, Korean Science and Engineering Foundation (KOSEF) through Center for Strongly Correlated Materials Research (CSCMR) at Seoul National University, and the BK21 program of the Ministry of Education. The work in Hanyang University was supported by Korea Research Foundation Grant (KRF-99-015-DI0040).

References

- [1] J.A.C. Bland, B. Heinrich (Eds.), *Ultrathin Magnetic Structures I*, Springer, Berlin, 1994.
- [2] B.T. Jonker, K.-H. Walker, E. Kisker, G.A. Prinz, C. Carbone, *Phys. Rev. Lett.* 57 (1986) 142.
- [3] N.C. Koon, B.T. Jonker, F.A. Volkening, J.J. Krebs, G.A. Prinz, *Phys. Rev. Lett.* 59 (1987) 2463.
- [4] D.P. Pappas, C.R. Brundle, H. Hopster, *Phys. Rev. B* 45 (1992) 8169.
- [5] Z.Q. Qiu, J. Pearson, S.D. Bader, *Phys. Rev. Lett.* 70 (1993) 1006.
- [6] A. Berger, H. Hopster, *Phys. Rev. Lett.* 76 (1996) 519.
- [7] D.M. Schaller, D.E. Bürgler, C.M. Schmidt, F. Meisinger, H.-J. Güntherodt, *Phys. Rev. B* 59 (1999) 14516.
- [8] C. Liu, E.R. Moog, S.D. Bader, *Phys. Rev. Lett.* 60 (1988) 2422.
- [9] J.G. Tobin, G.D. Waddill, D.P. Pappas, *Phys. Rev. Lett.* 68 (1992) 3642.
- [10] J. Thomassen, F. May, B. Feldmann, M. Wuttig, H. Ibach, *Phys. Rev.* 69 (1992) 3831.
- [11] D. Li, M. Freitag, J. Pearson, Z.Q. Qiu, S.D. Bader, *Phys. Rev. Lett.* 72 (1994) 3112.
- [12] S. Müller, P. Bayer, C. Reischl, K. Heinz, B. Feldmann, H. Zillgen, M. Wuttig, *Phys. Rev. Lett.* 74 (1995) 765.
- [13] M. Zharnikov, A. Dittschar, W. Kuch, C.M. Schneider, J. Kirschner, *Phys. Rev. Lett.* 76 (1996) 4620.
- [14] C.L. Fu, A.J. Freeman, *Phys. Rev. B* 35 (1987) 925.
- [15] R.E. Camley, D. Li, *Phys. Rev. Lett.* 84 (2000) 4709.
- [16] Z. Cellinski, B. Heinrich, J.F. Cochran, W.B. Muir, Z.S. Arrott, J. Kirschner, *Phys. Rev. Lett.* 65 (1990) 1156; O. Rader, E. Vescove, J. Redinger, S. Blügel, C. Carbone, W. Eberhardt, W. Gudat, *Phys. Rev. Lett.* 72 (1994) 2247.
- [17] S.-J. Oh, W. Kim, W. Kim, B.-H. Choi, J.-Y. Kim, H. Koh, H.-J. Kim, J.-H. Park, *Appl. Surf. Sci.* 169–170 (2001) 127.
- [18] B.N. Engel, C.D. England, R.A. Van Leeuwen, M.H. Wiedmann, C.M. Falco, *Phys. Rev. Lett.* 67 (1991) 1910.
- [19] D. Weller, W. Reim, K. Spörl, H. Brändle, J. Magn. Mater. 93 (1991) 183.
- [20] C. Liu, S.D. Bader, *J. Vac. Sci. Technol. A* 8 (1990) 2727.
- [21] C. Li, A.J. Freeman, H.J.F. Jansen, C.L. Fu, *Phys. Rev. B* 42 (1990) 5433.
- [22] C. Boeglin, H. Bulou, J. Hommet, X. Le Cann, H. Magnan, P. Le Fèvre, D. Chandesris, *Phys. Rev. B* 60 (1999) 4220.
- [23] X.F. Jin, J. Barthel, J. Shen, S.S. Manoharan, J. Kirschner, *Phys. Rev. B* 60 (1999) 11809.
- [24] C. Binns, C. Norris, G.P. Williams, M.G. Barthes, H.A. Padmore, *Phys. Rev. B* 34 (1986) 8221.
- [25] B. Heinrich, K.B. Urquhart, J.R. Dutcher, S.T. Purcell, J.F. Cochran, A.S. Arrott, D.A. Steigerwald, W.F. Egelhoff Jr., *J. Appl. Phys.* 63 (1988) 3863.
- [26] E. Mentz, D. Weiss, J.E. Ortega, A. Bauer, G. Kaindl, *J. Appl. Phys.* 82 (1997) 482.
- [27] H. Li, Y.S. Li, J. Quinn, D. Tian, J. Sokolov, F. Jona, P.M. Marcus, *Phys. Rev. B* 42 (1990) 9195.
- [28] D.E. Bürgler, C.M. Schmidt, D.M. Schaller, F. Meisinger, R. Hofer, H.-J. Güntherodt, *Phys. Rev. B* 56 (1997) 4149.
- [29] B.-Ch. Choi, S. Fölsch, M. Farle, K.-H. Rieder, *Phys. Rev. B* 56 (1997) 3271.
- [30] T.B. Massalski (Ed.), *Binary Alloys Phase Diagrams*, American Society for Metals, Metals Park, 1986.
- [31] P. Steiner, S. Hüfner, *Solid State Commun.* 44 (1982) 559.
- [32] J. Chastain, R.C. King Jr. (Eds.), *Handbook of X-ray photoelectron spectroscopy*, Physical Electronics, Eden Prairie, 1995.
- [33] B. Johansson, N. Mårtensson, *Phys. Rev. B* 21 (1980) 4427.
- [34] P. Steiner, S. Hüfner, N. Mårtensson, B. Johansson, *Solid State Commun.* 37 (1981) 73.
- [35] P. Steiner, S. Hüfner, *Acta Metall.* 29 (1981) 1885.
- [36] A.R. Miedema, P.F. de Châtel, F.R. de Boer, *Physica B* 100 (1980) 1.
- [37] R. Hultgren, R.L. Orr, P.D. Anderson, K.K. Kelley, *Selected Values of Thermodynamic Properties of Metals and Alloys*, Wiley, New York, 1963.

- [38] D. Briggs, M.P. Seah (Eds.), *Practical Surface Analysis*, Wiley, Chichester, 1983, p. 181.
- [39] M.P. Seah, W.A. Dench, *Surf. Interf. Anal.* 1 (1979) 1.
- [40] N. Mårtensson, R. Nyholm, B. Johansson, *Phys. Rev. Lett.* 45 (1980) 754.
- [41] H.P.J. Wijn (Ed.), *Magnetic Properties of Metals*, Springer, Berlin, 1991.
- [42] C.S. Shern, J.S. Tsay, H.Y. Her, Y.E. Wu, R.H. Chen, *Surf. Sci.* 429 (1999) L497.
- [43] P.M. Oppeneer, T. Maurer, J. Sticht, J. Kübler, *Phys. Rev. B* 45 (1992) 10924.
- [44] I. Osterloh, P.M. Oppeneer, J. Sticht, J. Kübler, *J. Phys. Condens. Matter* 6 (1994) 285.
- [45] G.Y. Guo, H. Ebert, *Phys. Rev. B* 51 (1995) 12633.
- [46] J.W. Cable, E.O. Wollan, W.C. Koeler, *Phys. Rev.* 138 (1965) A775.
- [47] G.G. Low, T.M. Holden, *Proc. Phys. Soc. London* 89 (1966) 119.